

Miniaturization of Inductively Coupled Plasma Sources

Y. Yin, J. Messier, and J. Hopwood
Department of Electrical and Computer Engineering
Northeastern University, Boston, Massachusetts 02115

The scaling laws associated with the miniaturization of planar inductively coupled plasmas (ICPs) are investigated. The applications for miniature ICPs include microelectromechanical systems (MEMS) for chemical analysis. Langmuir probe and microwave interferometry measurements of three ICPs with coil diameters of 5, 10, and 15 mm show that electron density typically falls in the range of 10^{16} - 10^{17} m^{-3} . The electron density is about an order of magnitude lower than large-scale ICPs as a result of the large surface-to-volume ratio of small discharges. The measured electron temperature is higher than predicted by a simple "global model" unless the plasma dimensions are determined more precisely by subtracting the sheath width from the chamber dimensions. Since the sheath width does not scale with the plasma size, the sheath width may ultimately limit the minimum size of ICPs. Plasma initiation power is determined to have a minimum at a gas pressure for which the electron collision frequency equals the frequency of the rf power supply. Small scale ICPs operating at 460 MHz can therefore be started most easily at ~ 1 Torr. The design of the coil is critical to miniature ICP performance. Unlike large-scale ICPs that operate efficiently using a broad range of coil shapes, the miniature coil must be carefully designed and constructed to minimize parasitic resistance.

I. INTRODUCTION

The demand for plasma processing equipment capable of uniformly treating large wafers has driven the development of larger plasma sources. The latest goal is the uniform plasma treatment of 300 mm diameter wafers which requires a plasma source diameter considerably larger than 300 mm. In this paper, however, we will describe the scaling-down of a plasma source to dimensions that are ultimately compatible with microelectromechanical systems (MEMS).

The desirable characteristics of a miniaturized MEMS plasma are similar to its large-scale counterparts. For example, the source should have the ability to operate using a reactive gas for long periods of time. This precludes small plasma sources that depend on electrodes or specially treated surfaces such as AC plasma displays.¹ In addition, the power dissipation should be minimal and the operating voltage should preferably be low and compatible with complementary metal-oxide-semiconductor (CMOS) circuits. An inductively coupled plasma is a reasonable choice since it is electrodeless and, with a characteristic input impedance of 50 Ω , requires only ± 10 V dc power supplies to deliver 1 W of rf power to the plasma.

Applications of miniaturized plasma sources include analytical instrumentation such as emission and mass spectroscopy. For example, Ross, *et al.*² have characterized a 9-mm inductively coupled microtorch for mass spectrometry. As analytical instruments are reduced in size and fabricated using MEMS technology, the need for MEMS-compatible sources of gas excitation and ionization is obvious. Another potential application of miniaturized plasma sources is the production of small ion beams used for the generation of thrust.³ For the analytical applications, it may be useful to operate the

plasma at relatively high pressures (10s of Torr), since miniaturized pumping systems will likely be inefficient at creating high vacuum environments. On the other hand, ion thruster applications will need plasma sources that operate at low pressure ($\sim 10^{-3}$ Torr) to insure efficient mass utilization. One of the goals of this work is to determine the scaling of operating pressure and plasma size for miniature inductively coupled plasmas.

In this paper three scaled-down ICPs are investigated with pancake-shaped coils of 5, 10 and 15 mm diameter. Large-scale ICPs typically operate by electrically resonating the coil at a frequency of 13.56 MHz. The optimum frequency for plasma generation is found to increase to 460 MHz as the coil diameter is reduced to 5 mm. The electron density produced by small ICPs is dependent on frequency, but the electron temperature and plasma potential are independent of frequency. This effect is attributed to the quality factor $Q(f)$ of the coil. The electron temperature is measured and found to compare favorably with a global model when the plasma dimensions are determined by subtracting the sheath width from the chamber dimensions. Since the sheath width does not scale, the limits of dimensional scaling will be determined by the plasma sheath.

II. EXPERIMENT

A. *Exploratory Scaling*

The initial attempt at a miniature ICP was formed from a 20-turn coil wound around a 6 mm Pyrex tube. The plasma was confined within the 4 mm i.d. of the tube. Two tungsten probes pierced the tube, allowing for the determination of electron temperature (T_e) and ion density (n_i) from the double Langmuir probe method.⁴ The

electron temperature was approximately 10 eV and the ion density $\sim 10^{10} \text{ cm}^{-3}$ using 1 Torr Ar and 3 W of 13.56 MHz power. A considerably more intense discharge could be generated at higher power, but even at 3 W the helical coil's excessive temperature limited plasma operation to a few minutes. In this configuration much of the power is dissipated in the coil rather than in the plasma. This is a common concern in large-scale ICPs as well⁵ since the power deposited in the plasma (P_{plasma}) is limited by the resistance⁶ of the plasma generating circuit (R_{system})

$$P_{plasma} = \frac{R_{plasma}}{R_{plasma} + R_{system}} (P_f - P_r) \quad (1)$$

where R_{plasma} is the resistance of the plasma, P_f is the forward power to the source, and P_r is the power reflected from the source. The efficiency of this preliminary plasma source was poor due to the large parasitic resistance of the 20-turn coil and large rf coil currents due to the low operating frequency.

B. Spiral Coil Design

The key to creating an efficient miniature ICP is controlling the resistance of the coil by designing a proper coil geometry and operating the ICP at the optimum frequency. In addition to improved efficiency, it is also desirable to use a planar-spiral coil since this shape is compatible with microfabrication techniques. The approach used to design the spiral coil was to choose a coil diameter and then optimize the number of turns, the gap between the turns, and the operating frequency such that the quality factor is maximized. The quality factor was determined from the ratio of the equivalent series reactance to the equivalent series resistance⁷ so that self-resonance effects are included. An approximate expression for the quality factor is

$$Q \approx \frac{2p f L_{TOT}}{R_{TOT}} \left[1 - \left(\frac{f}{f_R} \right)^2 \right] \quad (2)$$

where the resonant frequency (f_R) of the coil is

$$f_R = 1 / \sqrt{4p^2 L_{TOT} C_P} \quad (3)$$

As mentioned above, the total resistance of the coil should be minimized to achieve the best power transfer efficiency to the plasma. The total series resistance is comprised of three components

$$R_{TOT} = R_{DC} + R_{SE}(f) + R_{PE}(f) \quad (4)$$

which describe the DC resistance of the coil (DC), the skin effect (SE), and the proximity effect (PE) as

described in Snelling⁸ and Rodriguez, *et al.*⁷ The total inductance (L_{TOT}) of the coil is comprised of internal wire inductance, self inductance of each turn, and mutual inductance between turns. The parasitic capacitance (C_P) between coil turns is approximated from the capacitance between parallel conductors of cylindrical cross section. Both L_{TOT} and R_{TOT} are calculated by assuming the coil is constructed from interconnected concentric rings (see Ref. 7).

The theoretical quality factor for a typical 15 mm diameter spiral is shown in Fig. 1. The general trend is for $Q(f)$ to increase with frequency until self-resonance is approached. For the example shown, the highest quality factor occurs for $f = 100$ MHz. The plasma source built using this coil design operates between 100 MHz and 130 MHz.

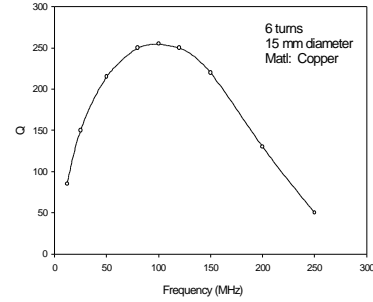


Fig. 1 - Calculated effective quality factor, $Q(f)$, for a 15 mm coil shows a maximum at 100 MHz before rolling off near self-resonance.

C. Miniature planar ICP sources

Spiral inductors were patterned on 1 oz. copper clad epoxy boards using photoresist and a contact mask aligner. The copper was spray etched using ferric chloride in water (1:3). This process resulted in a minimum line gap of approximately 100 μm in $\sim 30 \mu\text{m}$ thick copper. Thicker 2 oz. copper films were also used to construct the coils, but the minimum gap increased during the longer isotropic copper etch. As a result, the surface area of the coil was unchanged and no difference was observed in the performance of the ICP sources using 1 or 2 oz. copper. Two high voltage, high Q , variable capacitors provided the impedance matching of the rf power source ($Z = 50 \Omega$) to the plasma source. Figure 2 shows the top and bottom view of a complete ICP source. In addition to this 15 mm diameter source, two other coil sizes were investigated as detailed in Table 1.

The spiral coils were tested using a small vacuum system consisting of a stainless steel Tee as shown in Fig. 3. The coil was positioned adjacent to a 15 mm diameter window of 7056 glass with a thickness of 1.8 mm. Argon and air were introduced through a needle valve and the gas pressure was measured by a high accuracy capacitance manometer. Plasma power was controlled by a HP 8656A signal generator (1-990 MHz)

and amplified by a ENI 525LA 25 W linear amplifier. The forward and reverse power were monitored using a Narda 3020A dual directional coupler and a HP 435A power meter.



Fig. 2 - Top and bottom view of a miniature ICP circuit fabricated on a copper clad epoxy board. A U. S. dime is shown as a scale reference.

Optical and Langmuir probe diagnostics were introduced through a 1-1/3" conflat flange on the Tee opposite the plasma source. The single Langmuir probe was constructed from a tungsten wire (0.25 mm $f \times 4$ mm) that was sealed into the end of a 6 mm Pyrex tube. A second-order LC filter in series with the probe was tuned to the frequency of the power supply to eliminate rf distortion of the probe's current-voltage characteristic. The electron temperature (T_e) was determined from the slope of the $i-v$ curve in the electron retardation region after subtraction of the ion current. The plasma potential (V_p) was determined from the probe voltage at which $d^2i/dv^2 = 0$, and the electron density (n_e) was found from the electron saturation current at $v=V_p$.⁹ Probe measurements were not taken above ~ 0.5 Torr due to violation of the collisionless sheath assumption implicit in the data analysis. A 35 GHz microwave interferometer was used to confirm the Langmuir probe measurements by passing an electromagnetic wave across the plasma's diameter as shown in Fig. 3. The interferometer also allowed the average electron density to be determined at gas pressures above 0.5 Torr.

III. RESULTS AND DISCUSSION

A. Discharge appearance

Figure 4 shows photos of ICPs created by a 15 mm coil as viewed from the viewport opposite the coil. Photos (a) and (c) were taken at 0.02 Torr while (b) and (d) represent 1.4 Torr discharges. Both the argon and air

discharges appear diffuse and relatively uniform at pressures less than 1 Torr. Some interesting structure is visible in the plasma at higher pressures. The air plasma develops a ring-like shape characteristic of early inductive

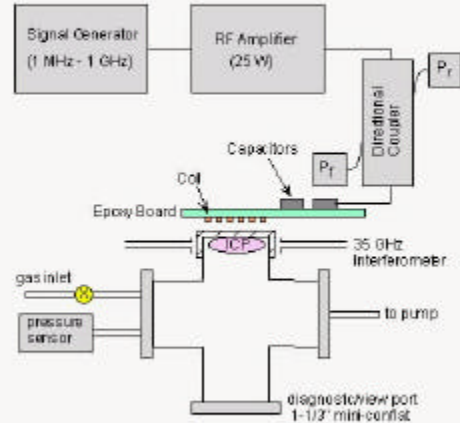


Figure 3

Fig. 3 - Schematic of the experimental system used to test miniature ICPs. The plasma diameter is 15 mm.

plasmas.¹⁰ The ring of plasma indicates that excitation occurs in the high electric field region created by the coil. At high pressure the plasma species de-excite before they can diffuse toward the center of the plasma. The ring structure is less evident in the 1.4 Torr argon plasma. At 10 Torr Ar, however, three small striations are observed to form around the chamber periphery. These striations appear similar to those reported by Stittsworth and Wendt in a 360 mm plasma at 0.085 Torr.¹¹

B. Plasma ignition

In MEMS applications the gas pumping speed is generally quite poor and a plasma source will need to operate at high pressure. Alternatively, in space applications the pumping of gas is not a problem, but because gas utilization is a concern, low pressure operation is important. These two applications point out the need to understand the parameters that effect plasma ignition as a function of pressure.

The relationship between the power supply frequency and the minimum power required to initiate a plasma is shown in Fig. 5. The chamber dimensions were not changed in this study, but the frequency was selected from 130 MHz, 220 MHz, or 460 MHz by reducing the coil diameter. At each operating frequency there is a gas pressure at which the plasma is most easily started. This minimum was found to occur when the electron elastic

collision frequency is approximately equal to the power supply's radian frequency ($\nu = \omega = 2\pi f$). The elastic collision frequency is computed from $\nu = K_{el} n_g$ where n_g is the argon gas density at room temperature ($3.5 \times 10^{22} \text{ m}^{-3}$ per Torr) and $K_{el} \sim 10^{-13} \text{ m}^3 \text{ s}^{-1}$ is the rate constant for elastic collisions with argon.¹² Arrows on Fig. 5 indicate the pressure at which $\nu = \omega$ for each operating frequency.

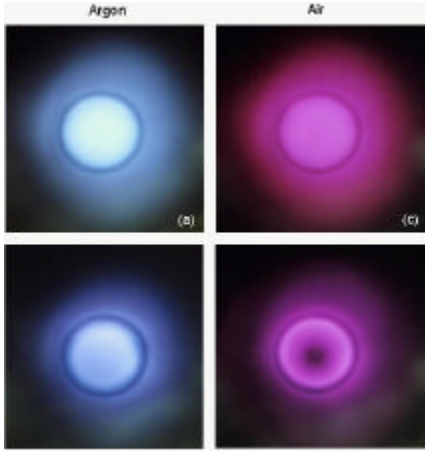


Fig. 4 - Photos of argon and air plasmas using 2 W rf at 0.02 Torr (top) and 1.4 Torr (bottom).

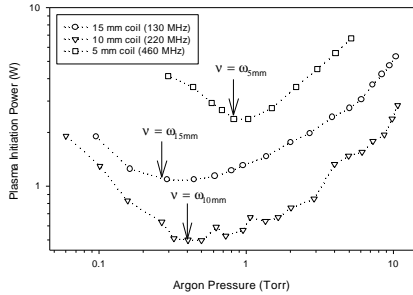


Fig. 5 - Power required for plasma ignition shows a distinct minimum versus pressure. The minimum occurs when the electron elastic collision frequency equals the source frequency ($\nu = \omega$) as shown by the arrows.

Because reduction of the coil diameter is accompanied by an increase in operating frequency, the ideal plasma ignition pressure will be 1-2 Torr for MEMS ICPs. The 5 mm coil did, however, require a higher total power to start the discharge compared to the larger coils. One reason higher power was needed is that the window thickness was not scaled with the coil diameter in this experiment. Ideally, the window thickness should be much less than the coil radius such that the inductive field strength does not decay too severely before reaching the window-plasma interface (see Ref. 5). Poor field penetration into the plasma region when the coil radius (2.5 mm) is comparable to the window thickness (1.8 mm) is a reason that the smallest ICP did not start as easily.

C. Electron density

Langmuir probe measurements of the electron density in a 0.14 Torr argon plasma are compared with the average electron density as determined by microwave interferometry¹³ in Fig. 6. The probe was located at the center of the discharge along the axis and sampled electrons from the 4 mm region nearest the coil. This central region is expected to yield the highest electron density when the plasma is diffuse at low pressure. The interferometer measures the line-integrated electron density (m^{-2}) across the diameter of the plasma which is then reported as average electron density (m^{-3}) after dividing by the plasma diameter. The error bar represents the uncertainty introduced by the minimum phase resolution of the interferometer.

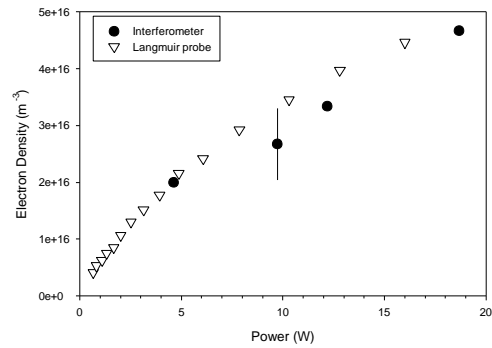


Fig. 6 - The electron density determined by Langmuir probe at the center of a 0.14 Torr argon discharge compares favorably with the average electron density as measured by microwave interferometry.

The plasma density determined by each technique is consistent, but it is approximately an order of magnitude less than large-scale ICPs.^{14,15} There are three explanations for the low electron density, (i) the surface area-to-volume ratio of the small plasmas is high, resulting in increased electron-ion wall recombination, (ii) the power efficiency is low due to resistive power loss in the coil, and (iii) the miniature plasmas may have a strong component of capacitive coupling that wastes rf power by accelerating charged species toward the coil rather than generating electron-ion pairs.

Although capacitive coupling cannot be conclusively eliminated as the cause of lower-than-expected density, a capacitively coupled discharge will exhibit a strong increase in rf floating potential with rf power as well as some dependence in the plasma potential. Probe measurements, however, show that the plasma potential, the electron temperature, and the rf component of the floating potential are essentially independent of rf power. Power efficiency of the coil is not quantified yet, but most of the power is absorbed by the plasma since the source can be operated continuously at several watts without excessive heating of the coil or

the tuning circuit. Finally, the surface-to-volume ratio of the current ICP is $\sim 4.5 \text{ cm}^{-1}$. In contrast, a typical large-scale ICP¹⁶ has a surface-to-volume ratio of only $\sim 0.3 \text{ cm}^{-1}$. This simple calculation shows that the surface recombination rate per unit plasma volume will be about an order of magnitude greater in the miniature ICP. This accelerated loss rate is believed to cause the order-of-magnitude decrease in electron density.

The electron density could not be determined at high pressure using the Langmuir probe since the collisional collection of charged particles is difficult to interpret. The average electron density as determined by interferometry, however, is shown in Fig. 7 up to a pressure of 5 Torr. Increased pressure results in higher electron density. This is an encouraging observation in the context of high pressure, scaled-down ICPs.

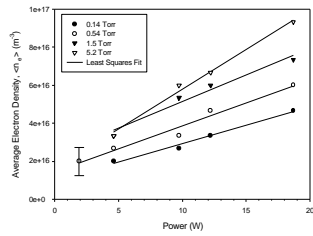


Fig. 7 - Microwave interferometry is used to determine the electron density in a miniature argon ICP at high pressure (coil diameter = 15 mm).

D. Electron temperature

The electron temperature in the miniature ICP is found to vary between 3 eV and 9 eV in argon. The usual, qualitatively observed increase in electron temperature occurs at both lower pressure and in smaller volume plasmas. To determine more general scaling laws for MEMS-compatible ICPs, the electron temperature data are plotted in Fig. 8 along with the global model¹⁷ for plasmas that is derived from particle balance. The global model states that the electron temperature is a unique function of gas density (n_g) and the effective plasma size (d_{eff})

$$\frac{K_{iz}}{u_B} \approx \frac{5 \times 10^{-14} e^{-15.7/T_e}}{\sqrt{kT_e / m_i}} = \frac{1}{n_g d_{eff}} \quad (5)$$

where the ionization rate constant for argon is K_{iz} ($\text{m}^3 \text{s}^{-1}$), u_B is the Bohm velocity, k is the Boltzmann constant and m_i is the argon ion mass. The effective plasma size has been determined in previous work from the radius (R) and length (L) of the plasma chamber,

$$d_{eff} = \frac{RL}{2(h_l R + h_r L)} \quad (6)$$

where h_l is the pressure-dependent ratio of the ion density at the top sheath edge to the ion density at the center of the plasma, and h_r is the ratio of ion density at the radial sheath edge to the center as described by Godyak.¹⁸ The raw data for the miniature plasmas *do not* follow the model described above *unless* the plasma sheath length is

subtracted from both R and L . The plasma sheath width (s) is determined from the Child Law

$$s = \frac{\sqrt{2}}{3} I_D \left(\frac{2V_P}{T_e} \right)^{3/4} \quad (7)$$

where I_D is the electron Debye length and V_P is the plasma potential. By making the substitutions $R \rightarrow (R - s)$ and $L \rightarrow (L - 2s)$, the measured electron temperatures are accurately predicted by the global model as shown. The subtraction of the sheath width is generally overlooked in large scale plasmas since the radius and length are much greater than s . In small scale discharges of this nature, the plasma dimensions are comparable to the sheath width ($\sim 1 \text{ mm}$). This results in an electron temperature that is somewhat higher than predicted on the basis of the chamber dimensions alone. The important general scaling principle revealed by this data is that the sheath width does not scale with the plasma size. In fact, since the electron density in smaller ICPs decreases, the sheath width becomes greater as the plasma is scaled down. A significant portion of the chamber volume may be occupied by the plasma sheath, resulting in a smaller than expected plasma volume and a higher electron temperature.

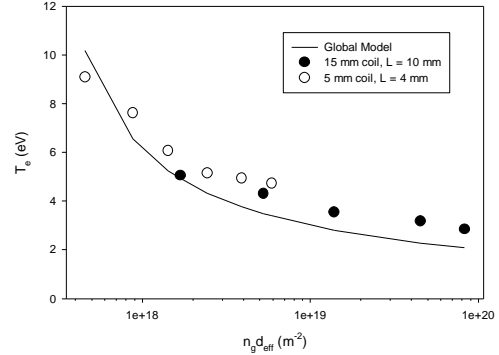


Fig. 8 - The measured electron temperature in two miniature ICPs agrees closely with the global model only when the size of the plasma is determined by subtracting the sheath width from the chamber dimensions.

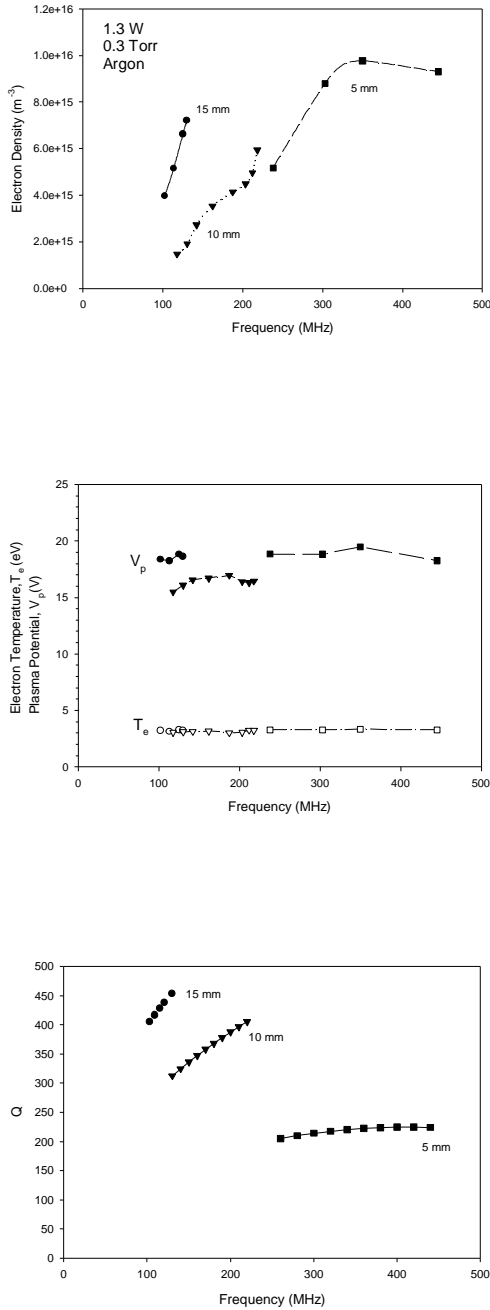


Fig. 9 - (a) The electron density determined by Langmuir probe shows a strong dependency on power supply frequency. (b) Since the electron temperature and plasma potential are independent of frequency, the ionization rate and energy loss rate are not frequency dependent. (c) The calculated quality factor for each coil shows that the efficiency of power coupling to the plasma improves at higher frequency. (Self-resonance is ignored, $C_p = 0$.)

E. Frequency effects

The excitation frequency of the miniature ICP is continuously varied from 100 MHz to 460 MHz in Fig. 9 by changing the capacitances used in the tuning network and decreasing the diameter (and inductance) of the coil. The upper frequency limit for each coil was reached when the reflected power (P_r) could no longer be nulled by tuning the capacitances. Fig. 9(a) shows the somewhat surprising result that the electron density increases with frequency. The increased electron density is not due to a higher ionization rate since the electron temperature remains constant as shown in Fig. 9(b). The energy loss rate from the plasma per electron-ion pair depends on the plasma potential (V_p). It can also be seen in Fig. 9(b) that V_p is approximately constant, and therefore the energy loss rate from the plasma is roughly independent of the frequency. Since generation and loss rates within the plasma are unaffected by frequency, the mechanism responsible for increased electron density must lie outside the plasma. One reason that the electron density improves with frequency is the efficiency of power coupling to the plasma (see Eq. 1.) The quality factor calculated for each coil, as plotted in Fig. 9(c), shows that the system resistance decreases with increasing frequency ($Q \sim 1/R_{system}$). As the frequency increases for each ICP, more power is available to the plasma as less is dissipated in the coil. Although further study is warranted, it appears from the data of Fig. 9 that the efficiency of the miniaturized ICP is strongly dependent on low-loss coil design and careful selection of the frequency.

IV. CONCLUSION

Planar inductively coupled plasma sources have been scaled-down, fabricated, and characterized. The smallest ICP uses a 5 mm diameter coil and operates at 460 MHz. The discharges have been tested in both argon and air over a pressure range from 0.01 Torr to 10 Torr. The plasmas can be initiated and sustained with as little as 0.5 W, but also operate as high as 20 W.

The primary scaling issues reported in this work are (i) the plasma starts most readily when $\nu = \omega$, (ii) the plasma sheath width does not scale-down, limiting the ultimate chamber dimension to be larger than the sheath width, (iii) the large surface-to-volume ratio of small ICPs decreases the electron density, and (iv) the plasma density is considerably more sensitive to the resistance of the coil circuit than large-scale ICPs.

Future work will focus on continued scaling of the coil diameter and reduction in the physical dimensions of the plasma chamber. To accomplish these goals, the source and chamber will be fabricated monolithically using MEMS fabrication techniques.

ACKNOWLEDGMENTS

The authors wish to thank Michael Miller, Richard Morrison, and Weilin Hu for their valuable

assistance. This work is funded by the National Science Foundation under Grant No. ECS-9701916.

Table 1. Parameters for the three miniature coils used in this work.

Coil diam. (mm)	Number of turns	Inductance (nH)	Width of the conductor (μm)	Gap between turns (μm)	Max. Q
5	3	36	200	100	240
10	5	200	200	200	290
15	6	720	450	140	260

REFERENCES

- ¹ R. M. Caloi and C. Carretti, "Getters and gettering in plasma display panels," *J. Vac. Sci. Technol. A*, vol. 16, pp. 1991-1996, 1998, (and refs. therein).
- ² B. S. Ross, D. M. Chambers, G. H. Vickers, P. Yang and G. M. Hieftje, "Characterisation of a 9-mm torch for inductively coupled plasma mass spectrometry," *J. Anal. At. Spectrom.*, vol. 5, pp. 351-358, 1990.
- ³ J. Mueller, J. R. Brophy, J. E. Polk, and J. J. Blandino, "The JPL ion thruster-on-a-chip concept," 7th NASA-OSAT Advanced Space Propulsion Workshop, Pasadena, CA, April 10, 1996.
- ⁴ M. A. Lieberman and A. J. Lichtenberg, *Principals of Plasma Discharges and Materials Processing*, New York: Wiley, 1994, p. 181.
- ⁵ J. Hopwood, "Planar rf induction plasma coupling efficiency," *Plasma Sources Sci. Technol.* vol. 3, pp. 460-464, 1994.
- ⁶ R. B. Piejak, V. A. Godyak, and B. M. Alexandrovich, "A simple analysis of an inductive RF discharge," *Plasma Sources Sci. Technol.*, vol. 1, pp. 179-186 1992.
- ⁷ R. Rodriguez, J. M. Dishman, F. T. Dickens, and E. W. Whelan, "Modeling of two-dimensional spiral inductors," *IEEE Trans. Components, Hybrids, and Manuf. Technol.*, vol. CHMT-3, pp. 535-541, 1980.
- ⁸ E. C. Snelling, *Soft Ferrites*, London: Iliffe, 1969.
- ⁹ B. Chapman, *Glow Discharge Processes*, New York: Wiley, 1980, pp. 60-70.
- ¹⁰ M. McKinnon, "On the origin of the electrodeless discharge," *Phil. Mag.* vol. 8, pp. 605-616, 1929.
- ¹¹ J. A. Stittsworth and A. E. Wendt, "Striations in a radio frequency planar inductively coupled plasma," *IEEE Trans. Plasma Sci.*, vol. 24, pp. 125-126, 1996.
- ¹² M. A. Lieberman and A. J. Lichtenberg, *Principals of Plasma Discharges and Materials Processing*, New York: Wiley, 1994, p. 80.
- ¹³ D. I. C. Pearson, G. A. Campbell, C. W. Domier, P. C. Efthimion, "A microwave interferometer for density measurement and stabilization in process plasmas," *Mat. Res. Soc. Symp. Proc.*, vol 117, pp. 311-317, 1988.
- ¹⁴ J. Hopwood, C.R. Guarnieri, S.J. Whitehair, and J.J. Cuomo, "Langmuir probe measurements in an rf induction plasma," *J. Vac. Sci. Technol. A*, vol. 11, pp. 152-156, 1993.
- ¹⁵ L. J. Mahoney, A. E. Wendt, E. Barrios, C. J. Richards, and J. L. Shohet, "Electron-density and energy distributions in a planar inductively coupled discharge," *J. Appl. Phys.*, vol. 76, pp. 2041-2047, 1994.
- ¹⁶ N. Forgotson, V. Khemka, and J. Hopwood, "Inductively coupled plasma for polymer etching of 200 mm wafers," *J. Vac. Sci. Technol. B*, vol. 14, pp. 732-737, 1996.
- ¹⁷ M. A. Lieberman and A. J. Lichtenberg, *Principals of Plasma Discharges and Materials Processing*, New York: Wiley, 1994, p. 306.
- ¹⁸ V. A. Godyak, *Soviet Radio Frequency Discharge Research*, Falls Church: Delphic, 1986, p. 99.